C_9N_4 as excellent dual electrocatalyst: A first principles study

Wei Xu(许伟), WenWu Xu(许文武), and Xiangmei Duan(段香梅)
Citation: Chin. Phys. B, 2021, 30 (**9**): 096802. DOI: 10.1088/1674-1056/ac0ccf
Journal homepage: http://cpb.iphy.ac.cn; http://iopscience.iop.org/cpb

What follows is a list of articles you may be interested in

Strain-tunable electronic and optical properties of h-BN/BC_3 heterostructure with enhanced electron mobility

Zhao-Yong Jiao(焦照勇), Yi-Ran Wang(王怡然), Yong-Liang Guo(郭永亮), and Shu-Hong Ma(马淑红)
Chin. Phys. B, 2021, 30 (**7**): 076801. DOI: 10.1088/1674-1056/abe29d

Two-dimensional PC_3 as a promising anode material for potassium-ion batteries: First-principles calculations

Chun Zhou(周淳), Junchao Huang(黄俊超), and Xiangmei Duan(段香梅)
Chin. Phys. B, 2021, 30 (**5**): 056801. DOI: 10.1088/1674-1056/abf10e

Selective linear etching of monolayer black phosphorus using electron beams

Yuhao Pan(潘宇浩), Bao Lei(雷宝), Jingsi Qiao(乔婧思), Zhixin Hu(胡智鑫), Wu Zhou(周武), Wei Ji(季威)
Chin. Phys. B, 2020, 29 (**8**): 086801. DOI: 10.1088/1674-1056/ab9438

Scalable preparation of water-soluble ink of few-layered WSe_2 nanosheets for large-area electronics

Guoyu Xian(冼国裕), Jianshuo Zhang(张建烁), Li Liu(刘丽), Jun Zhou(周俊), Hongtao Liu(刘洪涛), Lihong Bao(鲍丽宏), Chengmin Shen(申承民), Yongfeng Li(李永峰), Zhihui Qin(秦志辉), Haitao Yang(杨海涛)
Chin. Phys. B, 2020, 29 (**6**): 066802. DOI: 10.1088/1674-1056/ab889e

Effect of initial crystallization temperature and surface diffusion on formation of GaAs multiple concentric nanoring structures by droplet epitaxy

Yi Wang(王一), Xiang Guo(郭祥), Jiemin Wei(魏节敏), Chen Yang(杨晨), Zijiang Luo(罗子江), Jihong Wang(王继红), Zhao Ding(丁召)
Chin. Phys. B, 2020, 29 (**4**): 046801. DOI: 10.1088/1674-1056/ab790b

---

C_9N_4 as excellent dual electrocatalyst: A first principles study*

Wei Xu(许伟)[1], WenWu Xu(许文武)[1,2], and Xiangmei Duan(段香梅)[1,2,†]

[1] School of Physical Science and Technology, Ningbo University, Ningbo 315211, China
[2] Laboratory of Clean Energy Storage and Conversion, Ningbo University, Ningbo 315211, China

(Received 9 June 2021; revised manuscript received 9 June 2021; accepted manuscript online 21 June 2021)

We perform first principles calculations to investigate the catalytic behavior of C_9N_4 nanosheet for water splitting. For the pristine C_9N_4, we find that, at different hydrogen coverages, two H atoms adsorbed on the 12-membered ring and one H atom adsorbed on the 9-membered ring show excellent performance of hydrogen evolution reaction (HER). Tensile strain could improve the catalytic ability of C_9N_4 and strain can be practically introduced by building C_9N_4/BiN, and C_9N_4/GaAs heterojunctions. We demonstrate that the HER performance of heterojunctions is indeed improved compared with that of C_9N_4 nanosheet. Anchoring transition metal atoms on C_9N_4 is another strategy to apply strain. It shows that Rh@C_9N_4 exhibits superior HER property with very low Gibbs free energy change of -30 meV. Under tensile strain within $\sim 2\%$, Rh@C_9N_4 could catalyze HER readily. Moreover, the catalyst Rh@C_9N_4 works well for oxygen evolution reaction (OER) with an overpotential of 0.58 V. Our results suggest that Rh@C_9N_4 is favorable for both HER and OER because of its metallic conductivity, close-zero Gibbs free energy change, and low oneset overpotential. The outstanding performance of C_9N_4 nanosheet could be attributed to the tunable porous structure and electronic structure compatibility.

Keywords: C_9N_4 nanosheets, dual electrocatalyst, hydrogen evolution reaction, oxygen evolution reaction

PACS: 68.65.–k, 81.05.Rm, 71.15.Mb, 87.16.D– **DOI:** 10.1088/1674-1056/ac0ccf

1. Introduction

The scarcity of fossil fuels and the serious environmental pollution caused by their combustion make it urgent to develop renewable and clean energy alternatives.[1] Hydrogen, a renewable and clean energy with low emission, is expected to be one of the most ideal energy substitutes for solving environmental pollution.[2] Recently, hydrogen production by electrocatalytic hydrolysis has received widespread attention. Whether the catalyst promotes the activity of hydrogen evolution reaction (HER) and oxygen evolution reaction (OER) is a key factor in the electrocatalytic water splitting process.[3] So far, Pt has been regarded as an excellent catalyst for HER in the thermochemistry model of Nϕrskov.[4] Iridium oxide and ruthenium oxide are superior for the OER.[5] The high cost and low production hinder their extensive use. Currently, it is urgent to develop high performance, low cost, and suitable for widely used catalysts to promote the activity of HER and OER.

It has been known that adding heteroatoms and anchoring transition metals to carbon-based two-dimensional (2D) materials could significantly improve the catalytic activity of HER and OER.[6,7] In particular, single atom catalysts (SACs) on 2D sheets, with the coordination between anchored atoms and their surroundings, maximizes the performance and number of active sites.[8] For instance, Ni atom anchoring nitrogen-doped graphene exhibits good OER performance.[9] The heterojunction composed of N-doped graphene and g-C_3N_4 enhances HER activity,[10] and Mn atom anchored C_2N sheet shows good dual functions of OER and HER.[7] In view of the fact that most carbon nitride monolayers are semiconductors, used as HER catalyst, it is necessary to increase their conductivity by doping or anchoring metal atoms, and building heterojunctions. 2D materials composed of non-metallic elements with metallic characteristics will undoubtedly be ideal substitutes for precious metal materials.

Recently, a new type of carbon nitride porous nanosheet, C_9N_4, has been successfully predicted.[11] The good stability and unexpected conductivity of this flat structure open up a new way to explore non-metallic 2D materials. Based on the first principles calculations, we find that at certain hydrogen coverage, hydrogen atoms adsorbed on the 12-membered ring (H-tmr) and the 9-membered ring (H-nmr), show excellent property of the HER, even better than Pt. With the increase of the tensile strain applied to C_9N_4, the Gibbs free energy change (ΔG_{H^*}) reduce gradually. Especially, under the strain of 2%–6%, H-tmr at the coverage of 2/3 (tmr), the catalyst exhibits significant effect of HER. Further study shows that building heterojunctions, and/or anchoring Rh atom on C_9N_4 can indeed stretch the lattice and enhance the catalytic capability of HER. In addition, applying a tensile strain within 2% to Rh@C_9N_4 nanosheets, the HER activity is intentionally maintained or better. The heterojunctions composed by a lattice-matched 2D sheets and Rh@C_9N_4, can not only achieve extension, but also ensure that the value of ΔG_{H^*} is better than

*Project supported by the National Natural Science Foundation of China (Grant Nos. 11574167 and 11874033) and the K C Wong Magna Foundation in Ningbo University.

†Corresponding author. E-mail: duanxiangmei@nbu.edu.cn

that of Pt. With Rh atom as the active site, ΔG_{H^*} and the overpotential of OER is -0.03 eV and 0.58 V, respectively. Therefore, Rh@C_9N_4 has excellent electrocatalytic dual performance and provides a potential way for developing novel water splitting catalysts.

2. Computational method

All the computations are carried out by the spin-polarized density functional theory (DFT) using the projector augmented wave potentials which is operated in the Vienna *ab initio* Simulation Package (VASP).[12,13] A kinetic energy cutoff of 500 eV is used to set the plane-wave basis. The generalized gradient approximation contained in Perdew–Burke–Ernzerhof is employed to manage electron exchange-correlation.[14] The empirical correction method D3 is used to describe a damped van der Waals correction.[15] The Brillouin zones are sampled with $5 \times 5 \times 1$ Monkhorst–Pack meshes, and the van der Waals interaction based on Grimme's scheme (D3) is employed. A vacuum space of 20 Å along the z direction was added to avoid the artificial interaction between the periodic images. The convergence criterion for energy is set to be 10^{-5} eV, and the Hellmann–Feynman force of the atoms is less than 10^{-2} eV·Å^{-1}. The climbing-image nudged elastic band (CI-NEB) method is applied to obtain the diffusion barrier of HER and OER among the nearest stable sites.[16] Bader's charge population analysis is applied to calculate the atomic charge and electron transfer in different systems.[17]

The interaction between C_9N_4 and hybrid can be judged by the interfacial binding energy, E_b, which is defined as

$$E_b = E_{C_9N_4+\text{object}} - E_{C_9N_4} - E_{\text{object}},$$

where, $E_{C_9N_4+\text{object}}$, $E_{C_9N_4}$, and E_{object} represent the total energy of the complex, C_9N_4, and connected object (TM atom or the other 2D nanosheet), respectively. A more negative value of E_b shows a stronger thermodynamic stability.

A general criterion of the HER is applied to determine the process,[18] which is a multistep electrocatalytic process. The first step, namely the Volmer reaction, is the adsorption of the atomic hydrogen on the site, $H^+ + e^- + * \rightarrow H^*$, where the * represents the adsorption site of the catalyst. The subsequent step contains two possibilities: one is the Heyrovsky reaction, $H^* + H^+ + e^- \rightarrow H_2$, and the other is the Tafel reaction, $2H^* \rightarrow H_2$. The HER performance was evaluated by the Gibbs free energy change of forming adsorbed hydrogen (ΔG_{H^*}), in the step of the Volmer reaction: $H^+ + e^- + * \xrightarrow{\Delta G_{H^*}} H^*$. The near-zero ΔG_{H^*} of Pt (-0.09 eV) enables it to be powerful HER catalysts. At a standard conditions of pH = 0, $p(H_2) = 1$ bar (1 bar = 10^5 Pa), and U = 0 V, ΔG_{H^*} is obtained by[4,19]

$$\Delta G_{H^*} = \Delta E_{H^*} + \Delta E_{ZPE} - T\Delta S_H,$$

where ΔE_{H^*} is the adsorption energy of one H atom on C_9N_4, and equals

$$\Delta E_{H^*} = E_{\text{catalyst}+nH^*} - E_{\text{catalyst}+(n-1)H^*} - \frac{1}{2}E_{H_2},$$

ΔE_{ZPE} and ΔS_H represent the change of the zero-point energy and the entropy between the adsorbed state and gas phase, respectively. T is the temperature, and $T\Delta S_H$ is a constant value and taken as -0.20 eV.[4,20,21] ΔE_{ZPE} is obtained by[20]

$$\Delta E_{ZPE} = E_{ZPE}^{nH^*} - E_{ZPE}^{(n-1)H^*} - \frac{1}{2}E_{ZPE}^{H_2},$$

where $E_{ZPE}^{nH^*}$ represent the zero-point energy that n hydrogens adsorbed on the surface. $E_{ZPE}^{H_2}$ is the ZPE of H_2 in the gas phase.

The OER follows four elementary paths at the standard conditions of pH = 0, and $U = 0$ V,[7,22] and the free energy change ΔG of each path can be obtained according to the literature.[22] The overpotential η of OER (η^{OER}), an important criterion of the paths, is defined as the maximum of the four ΔG divide by e, then subtract oxygen reduction potential 1.23 V.[23]

3. Results and discussion

The optimized unit cell of C_9N_4 monolayer is a porous atomic lattice of 9- and 12-membered rings formed with C and N atoms. The lattice constant of C_9N_4 is computed to be 6.87 Å. The C–N bond length that connects the pentagon and makes up the pentagon is 1.30 Å, and 1.34 Å, respectively, and the C–C bond lengths of 9- and 12- membered rings are 1.56 Å and 1.45 Å, respectively, which are exactly the same with the corresponding values in the literature.[11] We calculate ΔG_{H^*} by adding one hydrogen atom after another to the sheet. The diffusion energy barrier of H atom from one adsorption point to the adjacent one is 1.04 eV, indicating that H is trapped and hard to move. We consider all the possibilities of H adsorbed on the 9- and 12-membered rings at different coverages.

For a single H atom adsorbed on C_9N_4, there are 3 equivalent sites to bind with N atoms in each cavity. The H-coverage, θ, is denoted as $n/3$ ($n = 1, 2, 3$). As listed in the left three columns of Table 1, when one H atom is adsorbed on the 12-membered rings (tmr) or the 9-membered rings (nmr), θ is 1/3, respectively. The coverage of 1/3 (nmr) shows a good hydrogen evolution performance, with a moderate and negative E_a and close to zero ΔG. However, for the coverage of 3/3 (tmr) and 2/3 (nmr), the positive E_a indicates that the adsorption of H atom is endothermic (will not be considered further). For the adsorption of H atoms on the 2×1 supercell, when θ is 1/3 (tmr) [*i.e.*, 2/6 (tmr) in the table] and 1/6 (nmr), the HER performance is excellent. As the supercell increased to be 2×2, for $\theta = 1/6$ [2/12 (tmr)], the hydrogen evolution performance is also acceptable. In order to find a strategy to improve the HER activity of C_9N_4, we mainly focus on the case

of $\theta = 2/3$ (tmr), with weak adsorption (-0.07 eV) and poor HER performance ($\Delta G = 0.33$ eV). Figure 1 shows their optimal structures with good hydrogen evolution performance. As illustrated in Fig. 2(a), the cases where the H coverage is less than 2/3 (tmr) show good hydrogen evolution performance, and some are even better than Pt.[4] Particularly, for two hydrogen atoms adsorbed on the 12-membered ring (2H-tmr) at 2/6 (tmr), ΔG_{H^*} is close to -0.02 eV, showing the excellent activity of HER. The catalytic performance of C_9N_4 can be improved by moderating the coverage of hydrogen.

Table 1. E_a (in unit eV), ΔG (in unit eV) of all the possibilities of H adsorbed on the 9- and 12-membered rings at different coverages.

θ-1×1	E_a	ΔG	θ-2×1	E_a	ΔG	θ-2×2	E_a	ΔG
1/3 (tmr)	–1.02	–0.62	1/6 (tmr)	–1.07	–0.67	1/12 (tmr)	–1.06	–0.66
2/3 (tmr)	-0.07	0.33	2/6 (tmr)	–0.42	–0.02	2/12 (tmr)	–0.46	–0.06
3/3 (tmr)	1.01	–	1/6 (nmr)	–0.33	0.07			
1/3 (nmr)	–0.31	0.09						
2/3 (nmr)	1.61	–						

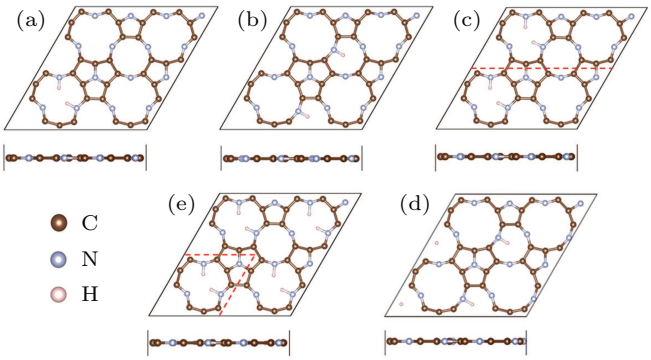

Fig. 1. The structure of hydrogen atoms absorbed at different hydrogen coverages (a)–(e): $\theta = 2/12$, 1/6, 2/6, 1/3, 2/3. Panels (a), (c), and (e) represent H adsorbed on the 12-membered ring (tmr). Panel (b) and (d) stand for H on the 9-membered ring (nmr).

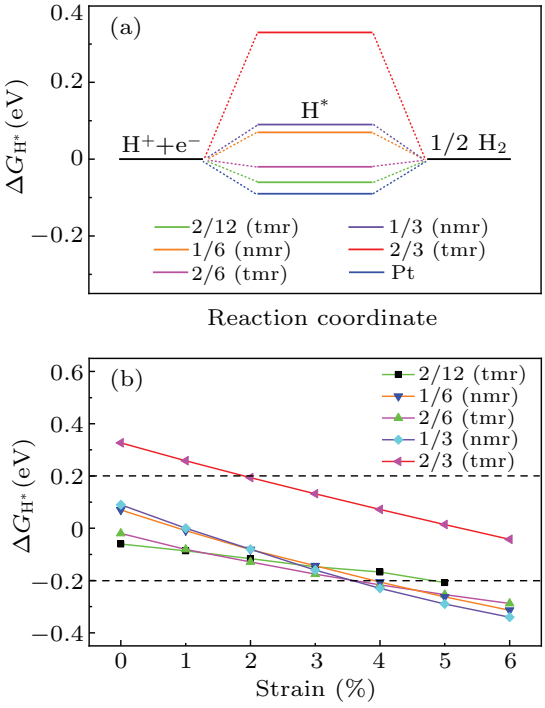

Fig. 2. (a) ΔG_{H^*} at different hydrogen coverages. ΔG_{H^*} of Pt was included for comparison. (b) ΔG_{H^*} as a function of the tensile strain.

Strain engineering has been proved to be an effective method for tuning the HER properties of 2D materials.[24,25] For the cases plotted in Fig. 2(a), ΔG_{H^*} under tensile strain are shown in Fig. 2(b). Within the tensile strain of 6%, the Gibbs free energy change decreases with the increase of strain. For the case of H atoms adsorbed on the 12-membered ring at $\theta = 2/3$ (tmr), the HER performance, the worst without strain (see Fig. 2(a)), is significantly improved at a strain range of 2% and 6%.

Stimulated by the report that the construction of heterojunction can regulate the structure and electrical properties, and improve HER performance.[20,26,27] We then consider to introduce BiN and GaAs to build heterojunction with C_9N_4 nanosheet, respectively. The lattice constants of BiN and GaAs are optimized to be 3.46 Å, 4.05 Å, respectively, which are consistent with the reported values of 3.47 Å, 4.06 Å.[28,29] The supercells of 2×2 of BiN and $\sqrt{3} \times \sqrt{3}$ of GaAs are combined with the unit cell of C_9N_4, and the lattice mismatch is 0.1%, 0.3%, respectively. The optimized lattice constant, binding energy and ΔG_{H^*} with 2H-tmr at hydrogen coverage of 2/3 (tmr) are listed in Table 2. For pristine sheet, ΔG_{H^*} equals 0.33 eV. BiN and GaAs sheets lead into a certain tensile strain to C_9N_4, and the values of $|\Delta G_{H^*}|$ are less than that of Pt, showing a good activity for hydrogen evolution. The negative values of E_b indicate good stability of the heterojunctions. In this work, we did find that applying tensile strain to C_9N_4 sheet can effectively regulate HER activity, and when the strain in the lattice-matched heterojunction is less than 1%, the HER performance is excellent. Such a small strain could be obtained in the experimental synthesis process. Comparable to the application of strain on the sheet alone, building a proper support to C_9N_4 could introduce a tensile strain, both the strain and the van der waals interaction between the heterostructure play a role on modulating the electronic property of the system. As a result of the synergy, the strain in the heterojunction is smaller than when the strain is applied alone. The density of states of junctions C_9N_4/BiN and C_9N_4/GaAs, are shown in Fig. 3. The pristine C_9N_4 nanosheet exhibits metallic property.[11] Note that all heterojunctions keep the metallic characteristic.

Table 2. The optimized lattice constant a (in unit Å), ΔG_{H^*} (in unit eV), and E_b (in unit eV) for C_9N_4 (denoted as CN) and the hybridizations.

System	a	ΔG_{H^*}	E_b	System	a	ΔG_{H^*}	E_b	System	a	ΔG_{H^*}	E_b
				Rh@CN	6.88	–0.03	–3.90				
CN	6.87	0.33	–	Pd@CN	6.90	0.16	–1.99	Rh@CN/Ge_3N	6.95	0.02	–0.42
CN/BiN	6.88	0.04	–0.62	Co@CN	6.88	0.39	–4.89	Rh@CN/InN	6.97	0.05	–0.26
CN/GaAs	6.89	–0.05	–0.59	Ni@CN	6.89	0.85	–4.18	Rh@CN/SnC	7.00	0.06	-0.12

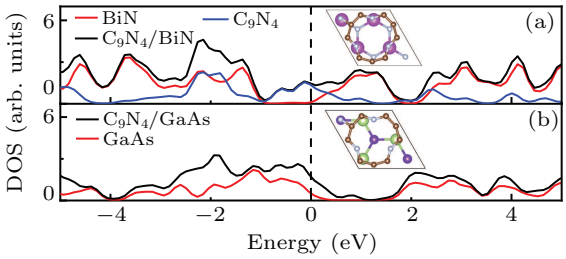

Fig. 3. The density of states for the junctions (a) C_9N_4/BiN, (b) C_9N_4/GaAs. The Fermi level is set at 0 eV.

Anchoring suitable transition metals (TM) on the allotrope of C_9N_4 has achieved remarkable effect on modulating the HER activity.[30] We anchor metal atom Co, Ni, Rh, and Pd to the 9- and 12-membered rings of C_9N_4 nanosheet, respectively. The tests show that the 9-membered ring is too small to load TM atoms intact. We therefore focus on putting the TM atom inside and outside the 12-membered ring, respectively. The configuration with a TM atom outside the cavity, bound to the three N atoms, is the most stable. As listed in Table 2, the lattice of C_9N_4 is indeed enlarged in the presence of TM atoms. The ΔG_{H^*} of H adsorbed on the Rh atom is as low as -0.03 eV, thus Rh@C_9N_4 is an outstanding catalyst for HER. To check whether a single metal atom prefers to be separated or aggregated on C_9N_4, the ratio of the binding energy to the bulk cohesive energy (E_b/E_{coh}) is calculated. Generally, E_b/E_{coh} greater than 0.5 indicates that the single atoms tend to be separated on the substrate, instead of gathering to clusters.[31,32] Take Rh@C_9N_4 as an example, the binding energy E_b between Rh and C_9N_4 is -3.90 eV, and the bulk cohesive energy of Rh is -5.8 eV.[33] The ratio of E_b/E_{coh} equals 0.67, which claims Rh atoms prefer to be anchored separately. Moreover, the diffusion energy barrier of Rh atom to the adjacent stable points is 2.1 eV, implying Rh atom bound stably at the initial site. The large binding energy and the high diffusion barrier prohibit the aggregation of metal atoms.

Strain has also been adopted to adjust the electronic interaction between metal and substrate.[34] We apply a small tensile strain to Rh@C_9N_4, and compare the ΔG_{H^*}, the d-band center and the binding energy with the unstrained case. The data are listed in Table 3, the absolute values of ΔG_{H^*} are less than 0.09 eV, implying that the catalyst is superior to Pt on the HER. Moreover, the d-band center, ε_d, of Rh is closer to the Fermi level with the increase of tensile strain, indicating the enhanced activity of the catalyst.[35] The binding energies of the strained cases keep large, which prevents the diffusion of Rh. As shown in Fig. 4, the conductivity of the strained systems remain as high as the unstrained case. The above results show that the Rh@C_9N_4 sheet has good ductility, under a tiny strain, its structural and electronic properties are robust, its catalytic activity is enhanced.

Table 3. ΔG_{H^*}, E_b, and d-band center ε_d between Rh and C_9N_4 nanosheets at the absence and presence of strain.

Strain (%)	ΔG_{H^*} (eV)	E_b (eV)	ε_d (eV)
0.0	-0.03	–3.90	–1.65
0.5	-0.01	–3.98	–1.61
1.0	0.01	–3.84	–1.55
1.5	0.03	–3.75	–1.49
2.0	0.05	–3.63	–1.44

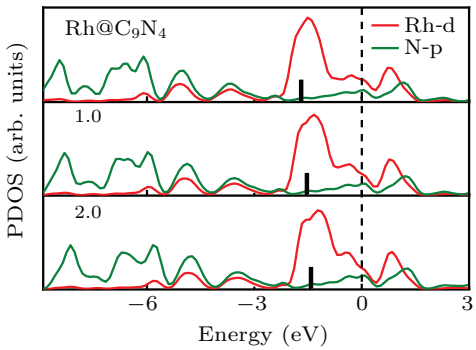

Fig. 4. PDOS of the p orbital of N with the d orbital of Rh at the absence and presence of strain, respectively. The Fermi level that is set at the zero and the d band center is marked by the vertical short black line, respectively.

In experiments, a big issue is how to accurately achieve such a small strain. The reported lattice constants of Ge_3N, InN, and SnC are 7.11 Å, 3.63 Å, and 3.60 Å,[29,36–38] respectively. It is possible to respectively combine the 2D sheet Ge_3N, InN, and SnC with Rh@C_9N_4, and their lattices match well. We explore to build a heterojunction using these 2D materials and Rh@C_9N_4. The lattice constants of Ge_3N, InN, and SnC are optimized to be 7.17 Å, 3.63 Å, and 3.60 Å, respectively, which are in good agreement with the literatures. The lattice mismatch between each of them and Rh@C_9N_4 is 1%, 1.3%, and 1.7%, respectively. The ΔG and the binding energy of the junctions are listed in Table 2. Amazingly, the Gibbs free energy change is basically consistent with the applied strain. The small negative value of E_b indicates that the interaction between the two components is weak van de Waals effect. We propose, to apply tiny tensile strain on Rh@C_9N_4 in the experiment, an effective and feasible method is to construct a junction with the Ge_3N, InN or SnC sheets.

The last but not least, we consider the Rh atom as the active site for oxygen evolution reaction. In order to get

the rate-determining step of OER on Rh@C_9N_4, we compute the change of free energy for each basic step. From Fig. 5, it can be obviously seen that the last step is the rate-determining step, and overpotential of OER (η^{OER}) is calculated to be 0.58 V. For the better evaluation of OER activity, we have compared more systems. For instance, the overpotential (η) of IrO_2 as OER catalyst is calculated to be 0.56 V. As the HER/OER bifunctional electrocatalyst, η is 0.52 V and 0.67 V for Ni@Mo_2B_2 and Mn@C_2N, respectively, and most of the M@C materials.[7,39–42] Based on the similar methodology, Rh@C_9N_4, as bifunctional electrocatalyst, exhibits good catalytic activity, and the value of HER/OER is −0.02 eV/0.58 V, respectively, indicating better HER/OER catalytic performance than Mn@C_2N (−0.15 eV/0.67 V).

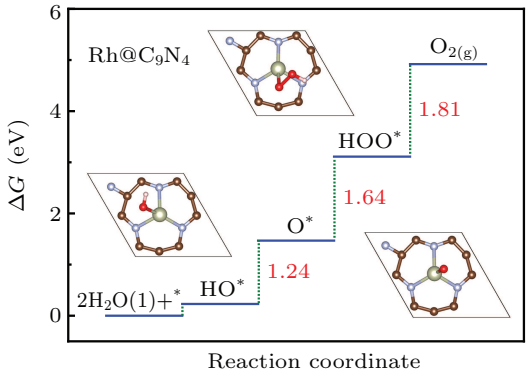

Fig. 5. Free energy diagram for OER on Rh@C_9N_4.

4. Conclusion

Using first principles calculations, we investigated the dual-performance of C_9N_4 nanosheet for water splitting. C_9N_4 nanosheet exhibits a metallic characteristic and shows excellent catalytic activity of HER with hydrogen atoms adsorbed on the 12-membered ring and the 9-membered ring, respectively. With the increasing tensile strain applied to C_9N_4, the Gibbs free energy change reduces gradually. Practically, constructing heterojunction with BiN or GaAs, and anchoring Rh atom on C_9N_4, could realize the tensile strain, the hybrid do promote the process of HER. For Rh@C_9N_4, the moderate tensile strain ($\sim 2\%$) may help to achieve the excellent effect of the HER as well. We demonstrate that it is a feasible way to introduce the tensile strain by building the heterojunctions between 2D sheets Ge_3N, InN or SnC and Rh@C_9N_4. ΔG_{H^*} of HER can be as low as −0.03 eV and the overpotential η^{OER} is 0.58 V, therefore, Rh@C_9N_4 emerges an excellent bifunction catalyst for both HER and OER. The C_9N_4 nanosheet is expected to open up a new way of high efficiency and promising dual-functional electrocatalysts for water splitting.

References

[1] Dresselhaus M S and Thomas I L 2001 *Nature* **414** 332
[2] Balat M 2008 *Int. J. Hydrogne Energ.* **33** 4013
[3] Mccrory C C L, Jung S, Ferrer I M, Chatman S, Peters J C and Jaramillo T F 2015 *J. Am. Chem. Soc.* **137** 4347
[4] Nørskov J K, Bligaard T, Logadottir A, Kitchin J R, Chen J G, Pandelov S and Stimming U 2005 *J. Electrochem. Soc.* **152** J23
[5] Lee Y, Suntivich J, May K J, Perry E E and Shaohorn Y 2012 *J. Phys. Chem. Lett.* **3** 399
[6] Liu X and Dai L 2016 *Nat. Rev. Mater.* **1** 16064
[7] Zhang X, Chen A, Zhang Z H, Jiao M G and Zhou Z 2018 *J. Mater. Chem. A* **6** 11446
[8] Tang L, Meng X, Deng D and Bao X 2019 *Adv. Mater.* **31** 1901996
[9] Fei H, Dong J, Feng Y, Allen C S, Wan C, Volosskiy B, Li M, Zhao Z, Wang Y and Sun H 2018 *Nat. Catal.* **1** 63
[10] Zheng Y, Jiao Y, Zhu Y H, Li L H, Han Y, Chen Y, Du A J, Jaroniec M and Qiao S Z 2014 *Nat. Commun.* **5** 3783
[11] Mortazavi B, Shahrokhi M, Shapeev A V, Rabczuk T and Zhuang X 2019 *J. Mater. Chem. C* **7** 10908
[12] Kresse G and Furthmuller J 1996 *Phys. Rev. B* **54** 11169
[13] Kresse G and Joubert D P 1999 *Phys. Rev. B* **59** 1758
[14] Perdew J P, Burke K and Ernzerhof M 1996 *Phys. Rev. Lett.* **77** 3865
[15] Grimme S, Antony J, Ehrlich S and Krieg H 2010 *J. Chem. Phys.* **132** 154104
[16] Henkelman G, Uberuaga B P and Jónsson H 2000 *J. Chem. Phys.* **113** 9901
[17] Henkelman G, Arnaldsson A and Jonsson H 2006 *Comp. Mater. Sci.* **36** 354
[18] Greeley J, Jaramillo T F, Bonde J, Chorkendorff I and Nørskov J K 2006 *Nat. Mater.* **5** 909
[19] Greeley J, Nørskov J K, Kibler L A, Elaziz A M and Kolb D M 2006 *ChemPhysChem* **7** 1032
[20] Yu S, Rao Y, Wu H and Duan X 2018 *Phys. Chem. Chem. Phys.* **20** 27970
[21] Gao D, Xia B, Wang Y, Xiao W, Xi P, Xue D and Ding J 2018 *Small* **14** 1704150
[22] Nørskov J K, Rossmeisl J, Logadottir A, Lindqvist L, Kitchin J R, Bligaard T and Jónsson H 2004 *J. Phys. Chem. B* **108** 17886
[23] Man I C, Su H, Callevallejo F, Hansen H A, Martinez J I, Inoglu N, Kitchin J R, Jaramillo T F, Nørskov J K and Rossmeisl J 2011 *ChemCatchem* **3** 1159
[24] Gao G, Sun Q and Du A 2016 *J. Phys. Chem. C* **120** 16761
[25] Gao G, Jiao Y, Ma F, Jiao Y, Waclawik E R and Du A 2015 *J. Catal.* **332** 149
[26] Geng S, Yang W and Yu Y S 2019 *J. Catal.* **375** 441
[27] Tang Y, Liu M, Zhou Y, Ren C, Zhong X and Wang J 2020 *J. Alloys Compd.* **842** 155901
[28] Zhou W, Zhang S, Guo S, Wang Y, Lu J, Ming X, Li Z, Qu H and Zeng H 2020 *Phys. Rev. Appl.* **13** 044066
[29] Zhuang H L, Singh A K and Hennig R G 2013 *Phys. Rev. B* **87** 165415
[30] Zhou Y, Gao G, Kang J, Chu W and Wang L 2019 *Nanoscale* **11** 18169
[31] Rao Y C, Peng Z, Li S F, Duan X M and Wei S H 2018 *Phys. Chem. Chem. Phys.* **20** 12916
[32] Huang J, Zhou C, Chu Z, Liu X and Duan X 2021 *Phys. Chem. Chem. Phys.* **23** 1868
[33] Changhyeok C, Seoin B, Na-Young K, Juhyung L, Yong-Hyun K and Yousung J 2018 *ACS Catal.* **8** 7517
[34] Zhu Y D, Zhao K, Shi J L, Ren X Y, Zhao X J, Shang Y, Xue X L, Guo H Z, Duan X M, He H, Guo Z X and Li S F 2019 *ACS. Appl. Mater. Inter.* **11** 32887
[35] Nørskov J K 1991 *Prog. Surf. Sci.* **38** 103
[36] Li Z, Yao Y, Wang T, Lu K, Zhang P, Zhang W and Yin J 2019 *Appl. Surf. Sci.* **496** 143730
[37] Sahin H, Cahangirov S, Topsakal M, Bekaroglu E, Akturk E, Senger R T and Ciraci S 2009 *Phys. Rev. B* **80** 155453
[38] Ma Y, Dai Y, Guo M, Niu C, Yu L and Huang B 2011 *Appl. Surf. Sci.* **257** 7845
[39] Cui X, Ren P, Deng D, Deng J and Bao X 2016 *Energ. Environ. Sci.* **9** 123
[40] Man I C, Su H Y, Calle-Vallejo F, Hansen H A, Martinez J I, Inoglu N G and Rossmeisl J 2011 *ChemCatchem* **3** 1159
[41] Zhang T, Zhang B, Peng Q, Zhou J and Sun Z 2021 *J. Mater. Chem. A* **9** 433
[42] Wang J R, Fan Y C, Qi S Y, Li W F and Zhao M W 2020 *J. Phys. Chem. C* **124** 9350